This is an open access article published under an ACS AuthorChoice License, which permits copying and redistribution of the article or any adaptations for non-commercial purposes.

BioMACROMOLECULES

pubs.acs.org/Biomac Article

Cellulose Mesh with Charged Nanocellulose Coatings as a Promising Carrier of Skin and Stem Cells for Regenerative Applications

Julia Pajorova,*,# Anne Skogberg,*,# Daniel Hadraba, Antonin Broz, Martina Travnickova, Marketa Zikmundova, Mari Honkanen, Markus Hannula, Panu Lahtinen, Maria Tomkova, Lucie Bacakova,* and Pasi Kallio*

Cite This: *Biomacromolecules* 2020, 21, 4857−4870

Read Online

ACCESS | Metrics & More | Article Recommendations | Supporting Information

ABSTRACT: Engineering artificial skin constructs is an ongoing challenge. An ideal material for hosting skin cells is still to be discovered. A promising candidate is low-cost cellulose, which is commonly fabricated in the form of a mesh and is applied as a wound dressing. Unfortunately, the structure and the topography of current cellulose meshes are not optimal for cell growth. To enhance the surface structure and the physicochemical properties of a commercially available mesh, we coated the mesh with wood-derived cellulose nanofibrils (CNFs). Three different types of mesh coatings are proposed in this study as a skin cell carrier: positively charged cationic cellulose nanofibrils (cCNFs), negatively charged anionic cellulose nanofibrils (aCNFs), and a combination of these two materials (c+aCNFs). These cell carriers were seeded with normal human dermal fibroblasts (NHDFs) or with human adipose-derived stem cells (ADSCs) to investigate cell adhesion, spreading, morphology, and proliferation. The negatively charged aCNF coating significantly improved the proliferation of both cell types. The positively charged cCNF coating significantly enhanced the adhesion of ADSCs only. The number of NHDFs was similar on the cCNF coatings and on the noncoated pristine cellulose mesh. However, the three-dimensional (3D) structure of the cCNF coating promoted cell survival. The c+aCNF construct proved to combine benefits from both types of CNFs, which means that the c+aCNF cell carrier is a promising candidate for further application in skin tissue engineering.

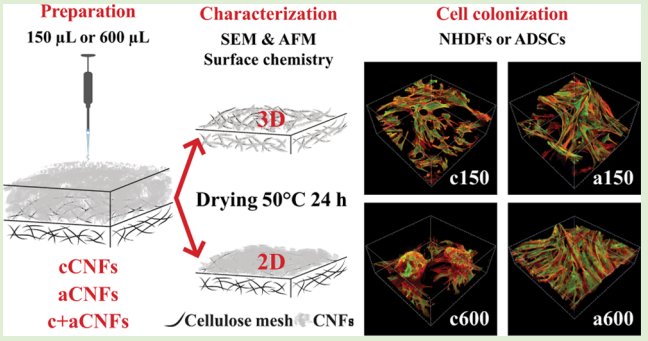

1. INTRODUCTION

Cellulose is frequently used in the production of biomaterials as a scaffold material to carry other molecules, supporting cell adhesion and promoting cell proliferation. Cellulose is an affordable biocompatible material that can be processed into cellulose nanofibrils (CNFs) and nanocellulose-based matrices with precisely controlled physical and chemical properties.

Wood-derived CNFs are manufactured from wood pulp using mechanical techniques alone or in combination with chemical and enzyme-assisted pretreatments.[1] The physico-chemical parameters of CNFs, such as swelling, are affected by hydrogen bonding and can be tuned by modifying the CNF dimensions or the charge density.[2,3] The common length of CNFs is within the micrometer range, whereas the width of CNFs is in the nanometer range,[2,4] which mimics the dimensions of extracellular matrix (ECM) components, such as collagen fibrils.[5] Moreover, CNFs form multiple types of solids, such as hydrogels, aerogels, and films with the stiffness range of the dermis and epidermis.[3] These materials absorb significant quantities of water, which is a desired property of wound dressings. The surface properties of wound dressings also have an effect on cellular behavior. The CNF surface has a weak negative charge in an aqueous solution in the unmodified form, which is not optimal for the growth of mammalian cells.[6] To enhance the cell−surface interactions, the CNF surface can be chemically modified to adjust the hydrophilicity or the surface charge, depending on the requirements of different cell types.[6−8] It has been reported that the modifications of CNFs with cationic or anionic functional groups promoted cell adhesion, proliferation,[6,9] cytocompatibility,[10,11] cell growth directionality,[12] water solubility, and bonding of other bioactive molecules,[7] such as collagen[13] and other peptides and proteins.[6] The beneficial effect of CNF hydrogels is especially emphasized in three-dimensional (3D) cell cultivation.[11,14,15] The application of CNFs as a wound dressing has also recently reached the clinical evaluation phase,[16] and it

Received: July 20, 2020
Revised: October 15, 2020
Published: November 2, 2020

Downloaded via TAMPERE UNIV on December 9, 2021 at 07:03:29 (UTC).
See https://pubs.acs.org/sharingguidelines for options on how to legitimately share published articles.

© 2020 American Chemical Society

https://dx.doi.org/10.1021/acs.biomac.0c01097
Biomacromolecules 2020, 21, 4857−4870

has been examined as a promising scaffold under *in vitro* conditions.[9,17,18]

There are two common chemical modifications that change the charge of the cellulose chain: (1) grafting of anionic 2,2,6,6-tetramethylpiperidine-1-oxyl (TEMPO) oxidation[19] and (2) grafting of cationic glycidyltrimethylammonium chloride (GTMAC).[6] The benefit of these modifications is in adjusting the desired surface properties of CNFs, e.g., for controlled adsorption of bioactive molecules, which can be further stabilized by cross-linking, driven by chemical functional groups introduced into the cellulose molecule.[7] TEMPO-mediated oxidation also allows low-energy mechanical disintegration of oxidized fibers.[19] TEMPO-oxidized anionic CNFs (aCNFs) promote cell adhesion and growth.[12] GTMAC-modified cationic CNFs (cCNFs) effectively adsorb negatively charged compounds,[10,20] including cell adhesion-mediating proteins,[6,21] mediate the binding and the release of hydrophobic drugs,[22] have an antimicrobial effect,[23] and facilitate cell attachment through electrostatic interactions.[8] The attachment of anchorage-dependent cells to CNFs is essential for a newly developed skin cell carrier. The cell adhesion can be regulated by modulating the roughness and the stiffness,[24,25] the surface chemistry,[24,26] the wettability,[3,27] or the electrostatic forces of the substrate.[26]

The present work enhances knowledge about the behavior of cells on promising charged CNF coatings of commercial, economical, and environmentally friendly cellulose meshes. To find an appropriate cell carrier for tissue engineering and wound healing applications, 3D and two-dimensional (2D) coatings of cationic (cCNF), anionic (aCNF), and combined (c+aCNF) nanocellulose were deposited on commercially available cellulose meshes. Since the proposed materials are to be used for skin applications, the CNF-coated meshes were tested *in vitro* with normal human dermal fibroblasts (NHDFs) and with hypodermal human adipose-tissue-derived stem cells (ADSCs).

2. MATERIALS AND METHODS

2.1. Production of Cellulose Nanofibrils. The CNF production and characterization were performed according to the study by Skogberg et al.[12] Both anionic and cationic CNF grades were produced from once-dried bleached birch kraft pulp. Anionic CNFs (aCNFs) were produced using TEMPO-mediated oxidation, as described by Saito et al.;[28] see Supporting Methods (S1.1). Cationic CNFs (cCNFs) were produced by introducing a positive charge using 2,3-epoxypropyl trimethylammonium chloride (EPTMAC; Raisacat, Chimagate, Lapua, Finland); the protocol is described in detail in our earlier study.[12] CNF materials were received from VTT Technical Research Centre (Espoo, Finland).

2.2. Preparation of CNF-Coated Meshes. PurCotton highly pure spunlace nonwoven cotton fabric (Winner Industrial Park, Shenzhen, China) was cut into 1.5 × 1.5 cm^2 samples (further referred to as "noncoated meshes"). The meshes were fixed into CellCrown inserts (Scaffdex Ltd., Tampere, Finland), which were inserted into 24-well cell culture plates (TPP, Trasadingen, Switzerland).

The CNF gels were diluted to a 0.15% (w/v) solution in Milli-Q water, sonicated for 2 min at 20% amplitude, and centrifuged at 10 000*g* for 60 min.[12] The CNF-coated meshes were prepared using either 150 or 600 μL of cCNF and aCNF supernatants (further referred to as "c150, c600, a150, a600") and by a combination of these supernatants (c+a), as described in Supporting Methods (S1.2). A pristine noncoated mesh was used as the control. The CNF-coated samples were dried for 24 h in a laboratory dryer (Binder, Tuttlingen, Germany) at 50 °C (Scheme 1). The sterilization included UV-C irradiation of both sides of the sample in a flow box for 20 min. The samples were sterilized twice in inserts in a sterile Petri dish before the CNF coatings were prepared and then after the CNF coatings had been dried.

Scheme 1. Schematic Picture of the Preparation of the Different Coating Topographies on the Cellulose Meshes Using cCNF and aCNF Solutions

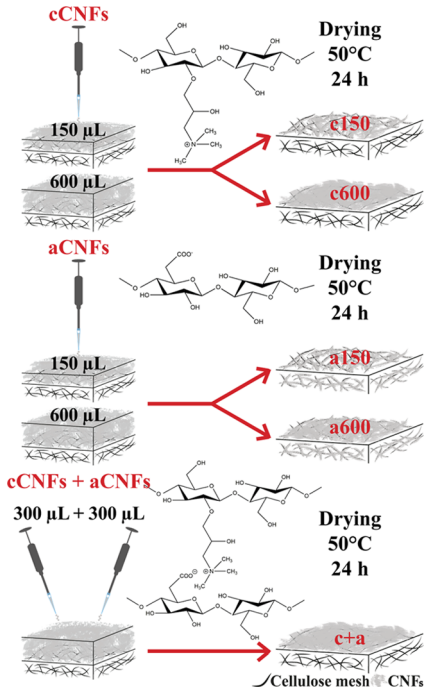

2.3. Characterization of the Noncoated and CNF-Coated Meshes. The CNF-coated meshes were characterized by scanning electron microscopy (SEM; Section 2.3.1) and atomic force microscopy (AFM; Section 2.3.3). Noncoated meshes were also imaged by microCT (S1.3). In addition, the physicochemical properties, i.e., the wettability (S1.4), the swelling ratio (Section 2.3.2), and the surface stiffness (Section 2.3.3), were studied.

2.3.1. Topography of CNF-Coated Meshes Using SEM. Front and side views of the CNF-coated meshes (c150, c600, a150, a600, and c+a) and noncoated meshes were acquired using SEM (ULTRAplus, Carl Zeiss, Oberkochen, Germany). The samples were attached to aluminum SEM stubs using a carbon tape and carbon-coated to avoid charging during the SEM studies. The front view was scanned from the surface of the CNF-coated or noncoated meshes, while the side view was scanned from the cut edges.

2.3.2. Swelling Ratio Measurements. The swelling ratio was measured either on a600, c600, and c+aCNF-coated and noncoated meshes ($n = 3$) or the corresponding glass coverslips (600 μL, $n = 3$). The initial dry weight (W_0) was measured before the samples were immersed in deionized water (dH_2O) or in Dulbecco's modified Eagle medium (DMEM) at 37 °C. The swollen samples were weighed (W_s) at two time points: after 20 min and after 20 h. After being weighed at time point 1 (20 min), the samples were returned into dH_2O or DMEM and incubated at 37 °C. The water uptake, subsequently referred to as the swelling ratio (SR), was determined as $SR = (W_s - W_0)/W_0$. The data was presented as the arithmetic mean ± standard deviation (SD) from three parallel samples for each experimental group.

2.3.3. Surface Mapping and Characterization of Mechanical Properties Using AFM. AFM data were acquired only for the samples coated with c600, a600, and c+a. The coatings were prepared by gradual application of 600 μL of CNF solution on both sides of the cellulose mesh. The first step is described in Supporting Methods (S1.2). 3D printed tubes fitted on the CellCrown inserts from the outer side were utilized for applying the CNF solution in the second

https://dx.doi.org/10.1021/acs.biomac.0c01097
Biomacromolecules 2020, 21, 4857−4870

step. Young's modulus and the surface arithmetic average roughness (R_a) were determined on the coating from the outer side of the samples. The samples in the inserts were mounted into a custom holder and mapped using an Olympus IX 81 camera (Japan) linked with a JPK NanoWizard 3 AFM microscope (JPK, Berlin, Germany).

Roughness maps of the dry samples were mapped in the hybrid acquisition mode (Quantitative Imaging mode, QI) with an SNL-10A probe (tip radius 2 nm, cantilever spring constant 0.361 N/m, sensitivity 15.4 nm/V; Bruker AFM Probes, Billerica, MA). QI images were acquired. The dry samples were further examined for their mechanical properties in the same setup as the roughness mapping but with an MPP-12120-10 probe (tip radius 8 nm, cantilever spring constant 5.05 N/m, sensitivity 13.1 nm/V; Bruker AFM Probes, Billerica, MA); for details, see Supporting Methods (S1.5).

The mechanical properties of the wet samples were probed at time points of 20 min and 17 h after immersion in Dulbecco's modified Eagle's medium (DMEM; Sigma-Aldrich Co., St. Louis, MO, Cat. no. D2902). In addition, the probe was replaced by a CP-qp-CONT-SiO colloidal probe (tip diameter 6.62 μm, cantilever spring constant 0.391 N/m, sensitivity 45.23 nm/V; NanoAndMore, Wetzlar, Germany); see Supporting Methods (S1.5).

All measurements were preceded by a calibration process. Two parallel samples (eight measurements in total) were used for each experimental group, and the data were presented as the median (Mdn) and the interquartile range.

2.4. Evaluation of Cell Behavior on CNF-Coated Meshes. Two cell types (Section 2.4.1) were cultured on meshes coated with each of the CNF coatings and on the noncoated meshes (Section 2.4.2) to compare the dependence of the cell behavior on the parameters of the sample. The proliferation (Section 2.4.3), the morphology (Section 2.4.4), and the protein-mediated adhesion (Sections 2.4.5, 2.4.6, and S1.12) of the cells were evaluated.

2.4.1. Cell Models and Culture Conditions. Neonatal normal human dermal fibroblasts (NHDFs, Lonza, Basel, Switzerland, Cat. no. CC-2509) were cultivated in the DMEM medium with 10% fetal bovine serum (FBS; Thermo Fisher Scientific, Gibco, Waltham, MA, Cat. no. 10270-106) and 40 μg/mL gentamicin (LEK, Ljubljana, Slovenia). Adipose-tissue-derived stem cells (ADSCs) were isolated from lipoaspirates after donors' confirmed written informed consent had been obtained, in compliance with the Declaration of Helsinki, and under ethical approval by the Ethics Committee at Na Bulovce Hospital in Prague. The isolation procedure for the ADSCs was performed according to Estes and co-authors,[29] with slight modifications as previously described.[30,31] The pooled ADSCs (for details, see Supporting Methods S1.6) were cultured in the DMEM medium and supplemented with 10% FBS, 40 μg/mL gentamicin, and 10 ng/mL recombinant human basic fibroblast growth factor (FGF2; GenScript, Piscataway, NJ).

2.4.2. Cultivation of Cells on CNF-Coated Meshes. The CNF-coated and noncoated meshes, fixed into CellCrown inserts and placed into 24-well cell culture plates (see above), were seeded with NHDFs and ADSCs in passage 3 at a density of 20 000 cells/insert (i.e., approx. 25 000 cells/cm^2) in 1 mL/well of the cell culture medium. An amount of 0.5 mL/well was added after 2 h of cultivation into the final volume of 1.5 mL/well. The cells were cultivated for 7 days in a cell incubator at 37 °C in a humidified air atmosphere with 5% CO_2. The behavior of the cells was evaluated in three time intervals (days 1, 3, and 7), and the culture wells of 24-well polystyrene plates (PS) were used as a control material.

2.4.3. Metabolic Activity of the Cells on CNF-Coated Meshes (Resazurin Assay). The level of metabolic activity of the NHDFs and ADSCs on cellulose meshes with all CNF coatings was measured as an indirect marker of the cell number in three time intervals (days 1, 3, and 7) using the conversion of resazurin sodium salt (Sigma-Aldrich Co., St. Louis, MO, Cat. no. R7017) into resorufin by mitochondrial enzymes (for details, see Supporting Methods S1.7). Four parallel samples were used for each experimental group and each time interval. The data were presented as the arithmetic mean ± standard deviation and were used for constructing growth plots to view the overall growth dynamics of the cells.

2.4.4. Fluorescence Staining and SEM Imaging of the Cells on CNF-Coated Meshes. The morphology of NHDFs and ADSCs seeded on the cellulose meshes with all CNF coatings was visualized in three time intervals (days 1, 3, and 7) by staining filamentous actin (F-actin) and vinculin, an important protein of focal adhesion plaques. Vinculin was stained to indicate the level of specific receptor-mediated cell adhesion and cell spreading. The detailed staining protocol and the imaging setup are presented in Supporting Methods (S1.8).

The morphology of the cells on the CNF-coated and noncoated meshes was further assessed by SEM on day 3 after cell seeding. The dehydrated samples, see Supporting Methods (S1.8) for details, were fixed on aluminum stubs using a carbon tape, followed by gold coating.

2.4.5. Protein Adsorption on CNF-Coated Meshes (Pierce BCA Protein Assay Kit). The investigated materials were preadsorbed with proteins derived from blood serum—FBS or bovine serum albumin (BSA)—which modulate the cell adhesion. The total amount of these proteins adsorbed on the CNF-coated (c600, a600, c+a) and noncoated meshes was evaluated by the Pierce BCA Protein Assay Kit (Pierce BCA Protein Assay, Rockford, IL); for details, see Supporting Methods (S1.9). Four parallel samples (eight measurements in total) were used for each experimental group, and the data were presented as the arithmetic mean ± standard deviation of the adsorbed proteins (mg/sample), calculated from the BSA calibration curve according to the manufacturer's protocol. The data were further expressed as the ratio of the adsorbed proteins (mg/sample) to the concentration of the total proteins in 1.5 mL of added FBS and BSA solutions and given as a percentage.

2.4.6. Cell Adhesion on cCNF Coatings Preadsorbed with Proteins. To explain the cell behavior on cCNF coatings, meshes (see S1.10) and glass coverslips (see S1.11) with cCNF coatings were used for evaluating the dependence of the cell adhesion on the composition of the preadsorbed proteins. The initial cell adhesion on the c600 coatings was observed by fluorescence staining of the cells, as described above (Section 2.4.4). The treated group of cCNF coatings was preadsorbed with proteins for 2 h before cell seeding, while the cCNF coating control group was seeded with cells and proteins simultaneously (Scheme S1).

2.5. Statistical Analysis. The statistical significance of the data measured by AFM was evaluated using the nonparametric analysis of variance (Kruskal–Wallis), with Tukey's posthoc test for pairwise comparison. Values of $p \leq 0.05$ were considered significant. If not stated otherwise, the data postprocessing and statistical testing were performed in Matlab 2019a (MathWorks Inc., Natick, MA). The parametric data from the measurements of the swelling ratio, the cell metabolic activity, and the protein adsorption were evaluated using parametric analysis of variance (ANOVA) with Tukey's posthoc test for pairwise comparison. Values of $p \leq 0.05$ were considered significant.

3. RESULTS

3.1. Structural Characterization of the Noncoated and CNF-Coated Meshes. According to the MicroCT analysis (Figure S1), the average fiber thickness of the noncoated mesh was 7.2 ± 1.97 μm (max. 16.1 μm), while the average void thickness was 44.3 ± 36.3 μm. The noncoated mesh possessed high porosity of 84.9%.

The topography of the noncoated and CNF-coated meshes was analyzed using SEM (Figure 1). Depending on the volume applied on the surface of the cellulose mesh and on the charge of the CNFs, the CNF solutions either penetrated into the pores of the mesh, mimicking the 3D structure of the mesh, or formed an almost flat layer on top of the mesh (Figure S1). The CNF solutions with a volume of 150 μL (a150, c150) covered the individual fibers of the mesh and filled the pores between them (see the first column in Figures 1 and S1), while a volume of 600 μL (c600, a600) formed a thin film on the

https://dx.doi.org/10.1021/acs.biomac.0c01097
Biomacromolecules 2020, 21, 4857−4870

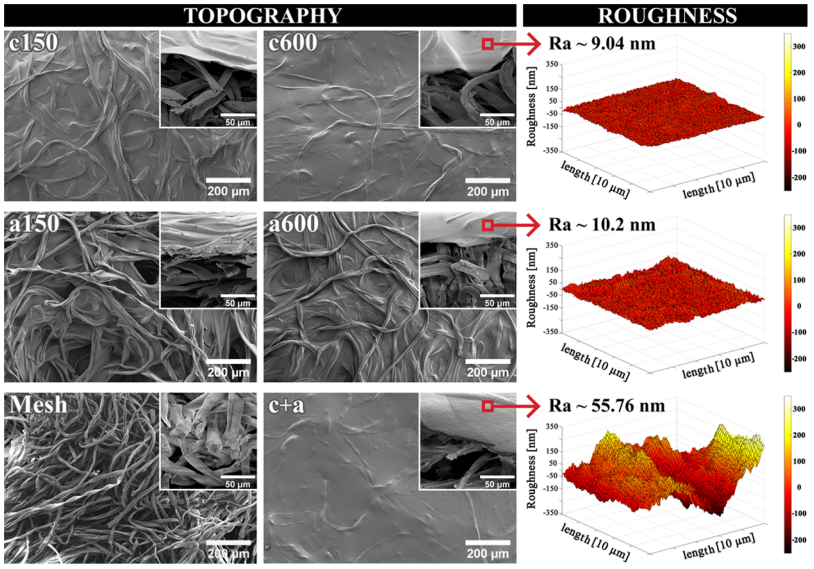

Figure 1. Topography and roughness. Front view and side view (inset image) of SEM images of c150, c600, a150, a600, and c+aCNF-coated and noncoated meshes (left and center). The roughness of the c600, a600, and c+aCNF-coated meshes was measured by AFM (right).

surface of the mesh (see the second column in Figures 1 and S1). At the same time, the cCNFs, mainly c600 and c+a, showed a tendency to form a flat, 2D film-like coating on the mesh surface, while the aCNFs, predominantly a150, covered the individual mesh fibers and filled the pores between them, which created a more pronounced 3D microtopography. As a result, the best-developed 3D microtopography was obtained using 150 μL of aCNFs, and the most pronounced film-like 2D microtopography was observed when 600 μL of cCNFs or c+aCNFs was used (Figures 1 and S1).

The surface roughness was determined using AFM. The results show that the R_a median of a600 was 9.04 nm and the R_a median of c600 was 10.20 nm The R_a median of c+a was 55.76 nm (Figure 1). Groups c600 and a600 were significantly different from group c+a (p = 0.025) (Figure S1).

3.2. Swelling Ratios and Contact Angles of CNF Coatings. The swelling ratios of the noncoated and c600, a600, and c+aCNF-coated meshes were determined after 20 h in deionized water (dH_2O) and DMEM. The highest swelling ratio was measured in dH_2O in the c600 coatings. However, there was no significant difference between CNF-coated and noncoated meshes in DMEM (Figure 2A). Due to the considerable water uptake of the underlying meshes, the CNF coatings were prepared on glass coverslips and the swelling ratio in DMEM was measured (Figure 2B). The swelling ratio of the c600 coatings was significantly higher than those of the a600 and c+a coatings after 20 min in DMEM, but after 20 h, there was no additional water uptake by the c600 coatings (Figure 2B). However, the water uptake by the a600 coatings increased with time, and the values after 20 h were significantly higher (p = 0.03) than the values after 20 min (Figure 2B). The swelling ratio of the c+a coatings increased slightly between 20 min and 20 h (Figure 2B). The swelling ratios of the noncoated meshes in DMEM and dH_2O were comparable (Figure 2A), and they remained relatively unchanged during the incubation period in DMEM (Figure 2B). The measured contact angles are reported in the Supporting Information (Figure S2).

3.3. Stiffness of the CNF Coatings Measured Using AFM. The average stiffness values (arithmetic mean ± SD) of c600, a600, and c+aCNF-coated meshes in the dry state were 0.572 ± 0.24 GPa (Mdn = 0.640), 0.683 ± 0.45 GPa (Mdn = 0.538), and 0.315 ± 0.10 GPa (Mdn = 0.275), respectively. Although there was a significant difference in coating stiffness between a600 and c+a (p = 0.034), the mean Young moduli reached the same order of magnitude, and the confidence interval demonstrated only a negligible difference (Figure 2C).

The average stiffness values of the CNF-coated meshes after wetting in DMEM for 20 min were 121 ± 16 kPa (Mdn = 116), 342 ± 101 kPa (Mdn = 326), and 241 ± 83 kPa (Mdn = 230) (Figure 2D—0 h). Young's moduli in the wet state (Figure 2D) are, on an average, three orders of magnitude lower than that in the dry state (Figure 2C), which indicates considerable softening of the materials after wetting. The c600 coatings were significantly (p = 0.002) softer than the a600 coatings, while the stiffness of the c+a coatings was between them after 20 min in DMEM (Figure 2D, 0 h).

The average stiffness values of the CNF-coated meshes after 17 h in DMEM were 131 ± 37 kPa (Mdn = 121), 173 ± 117 kPa (Mdn = 194), and 219 ± 174 kPa (Mdn = 221), respectively (Figure 2D, 17 h). Although the median values of a600 and c+a stiffness were higher than the c600 stiffness values, no significant difference between the tested groups was found (Figure 2D, 17 h). There was a significant difference (p = 0.034) within the a600 coatings, depending on the time scale, while Young's moduli of the c600 (p = 0.999) and c+a (p = 0.848) coatings did not differ significantly after 17 h from the situation after 20 min. The stiffness of the a600 coatings decreased with time (Figure 2C), while the water uptake increased with time (Figure 2A), which means that a600 coatings become softer during incubation in DMEM.

3.4. Cell Behavior on CNF-Coated Meshes. *3.4.1. Overall Growth Dynamics of Cells on CNF-Coated Meshes.* The growth of NHDFs and ADSCs on the CNF-coated and noncoated meshes was evaluated at three time intervals by measuring the cell metabolic activity using the resazurin assay. The values of the cell metabolic activity—an indicator of the cell number—were used for constructing growth plots to evaluate the overall growth dynamics of the cells within a 1-week period (Figure S3).

https://dx.doi.org/10.1021/acs.biomac.0c01097
Biomacromolecules 2020, 21, 4857−4870

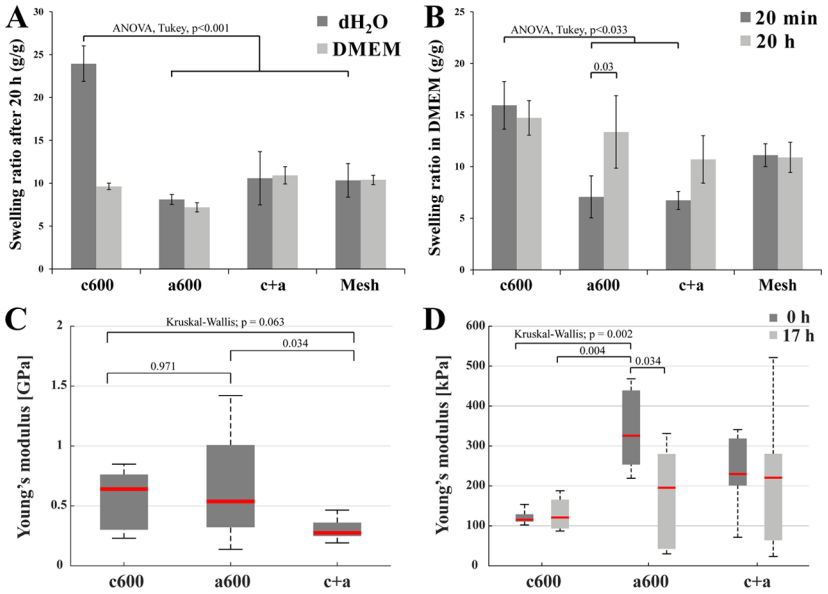

Figure 2. Swelling ratio and stiffness. Swelling ratio of CNF-coated meshes after 20 h in dH_2O and DMEM (A). Swelling ratio of CNF-coated glass coverslips after 20 min in DMEM and after 20 h in DMEM (B). Arithmetic mean ± SD from three independent samples, ANOVA, Tukey's method, and statistical significance ($p \leq 0.05$). Young's modulus before wetting with DMEM (dry state; C) and after wetting with DMEM (wet state; 0 h; 17 h; D). Median and interquartile range from eight measurements, Kruskal–Wallis, Tukey's method, and statistical significance ($p \leq 0.05$).

The dynamics of the cell growth on meshes coated with aCNFs or c+aCNFs were comparable to the dynamics on standard tissue culture PS, while on the cCNF-coated meshes, it was similar to the dynamics on the noncoated meshes. Interestingly, these differences were more apparent in NHDFs than in ADSCs (Figure S3). This motivated a deeper analysis of the mechanisms behind these phenomena. The initial adhesion of the two cell types on the CNF-coated and noncoated meshes (Figure 3) and the adsorption of serum-derived proteins (Figure 4) were characterized on day 1 after cell seeding. The proliferation and the morphology of the cells were observed on day 3 when the cells were fully spread and their morphology was well developed (Figures S5 and 5). The final status of the colonization of the CNF-coated cellulose meshes with cells was evaluated on day 7 (Figures S6 and 6).

3.4.2. Day 1: Initial Adhesion of Cells on CNF-Coated Meshes. We observed that the metabolic activity and the morphology of the NHDFs and the ADSCs on the cCNF-coated and aCNF-coated meshes differed (Figure 3). The metabolic activity of the NHDFs was significantly lower on the cCNF coatings than that on the aCNF and c+aCNF coatings (Figure 3A). Conversely, the metabolic activity of ADSCs on the cCNF coatings was mostly similar to, or even slightly better than, on the aCNF coatings (Figure 3B). The cell metabolic activity of both cell types on c+a coatings reached almost the same level as on polystyrene (PS = 100%; Figure 3A,B).

Similarly, the visualization of the cell morphology revealed that NHDFs on c600 coatings was often rounded and nonspread (Figure 3C), while the adhesion and spreading of ADSCs were almost the same as those on the a600 and c+a coatings (Figure 3D). The 3D topography of the a150 CNF-coated meshes supported the attachment and physiological elongation of both cell types. The flat c600, a600, and c+a coatings were more suitable for cell spreading into a polygonal shape, as they provided the cells with a more homogeneous flat area (Figure 3C,D). Vinculin was homogeneously dispersed throughout the cells, and no distinct focal adhesion sites were observed in the cells on any type of the CNF coating (Figure 3C,D), even at higher magnification (objective 40×; data not shown).

3.4.3. Day 1: Adsorption of Serum-Derived Proteins on CNF-Coated Meshes. To explain the differences in the initial cell attachment and spreading on the CNF-coated meshes on day 1, c600, a600, c+a and noncoated meshes were preadsorbed with serum-derived proteins modulating cell adhesion (Figure 4). When the samples were pretreated with 1.5 mL of 10% FBS in DMEM, a significantly greater amount of proteins was adsorbed on the c600 and c+a coatings than that on the a600 coatings and on the noncoated meshes (Figure 4A). To estimate the adsorption of non-cell-adhesive BSA from 10% FBS, the samples were pretreated with 1.5 mL of 0.25% BSA in DMEM, which theoretically corresponds to the average concentration of BSA in 10% FBS. Interestingly, the absolute amount of adsorbed BSA on the c600 coatings was lower than that of the absolute amount of proteins adsorbed from 10% FBS (Figure 4A). However, the percentage of BSA (15.6%) adsorbed on c600 from the BSA solution was higher than the percentage of proteins (13.1%) adsorbed from 10% FBS (Figure 4B). In contrast, the percentage of BSA (5.5%) adsorbed from the BSA solution on the a600 coatings was lower than that of the percentage of proteins (6.9%) adsorbed from the 10% FBS (Figure 4B). On the c+a coatings, the BSA (12.4%) adsorbed from the BSA solution in a similar proportion to the proteins (12.5%) adsorbed from the 10% FBS (Figure 4B). These results indicate that the c600 and c+a coatings adsorbed more non-cell-adhesive BSA from the FBS than the a600 coatings and noncoated meshes adsorbed. This may explain the lower cell adhesion on the cCNF coatings than that on the aCNF coatings.

3.4.4. Day 1: Adhesion of Cells on cCNF Coatings preadsorbed with Serum-Derived Proteins. Due to the differences in attachment between the cells on cCNFs (Figure

https://dx.doi.org/10.1021/acs.biomac.0c01097
Biomacromolecules 2020, 21, 4857−4870

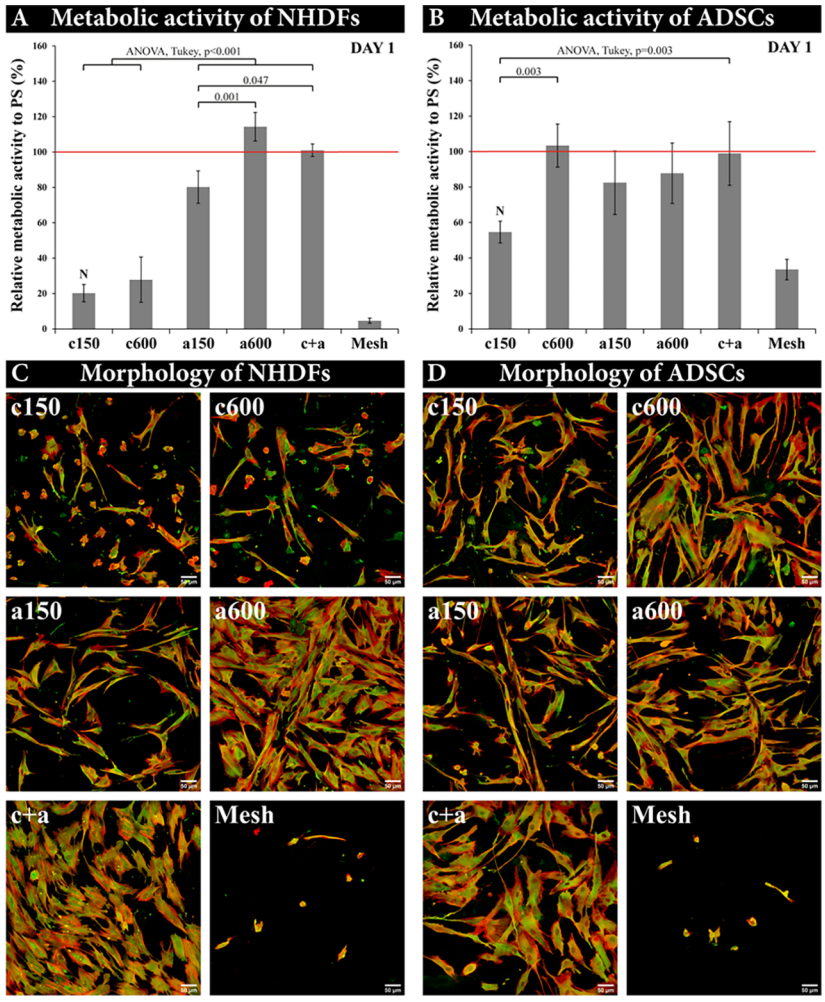

Figure 3. Metabolic activity (A, B) and the morphology (C, D) of NHDFs and ADSCs on CNF-coated and noncoated meshes on day 1 after cell seeding. (A, B) Metabolic activity of the cells on CNF-coated and noncoated meshes is displayed as a value relative to the metabolic activity of the cells on polystyrene (PS = 100%; red lines). Arithmetic mean ± SD from eight measurements made on four independent samples, ANOVA, Tukey's method, and statistical significance ($p \leq 0.05$). N, No significant difference in comparison with the noncoated mesh (mesh). (C, D) F-actin in the cell cytoskeleton is stained in red and vinculin is stained in green. A confocal microscope with an objective magnification of 20×. Scale bar = 50 μm.

3) and due to the adsorption of the serum-derived proteins predominantly on the cCNFs (Figure 4A,B), the initial adhesion of cells on preadsorbed serum-derived proteins was studied only on the cCNF coatings.

On the cCNF-coated meshes preadsorbed with FBS, the ADSCs and NHDFs adhered in low numbers, and their shape after 24 h was abnormal and nonphysiological (Figure 4C,D). However, when the cells were seeded in DMEM supplemented with FBS on pure cCNF-coated meshes, the adhered ADSCs were almost confluent and were well-spread after 24 h. In contrast, the number of adhered NHDFs remained low, and their morphology was comparable with the NHDFs on the cCNF coatings preadsorbed with FBS. Similar results were observed in BSA, although this protein is nonadhesive for cells. On meshes preadsorbed with BSA, both cell types were unable to spread after 2 h. However, when the cells were seeded on pure cCNF-coated meshes in DMEM supplemented with BSA, the ADSCs adhered in greater numbers than the NHDFs and showed some tendency to spread after 2 h of cultivation (Figure 4C,D).

In addition to the investigation into cCNF-coated meshes, the response of NHDFs and ADSCs to the preadsorbed proteins was investigated on cCNF-coated glass coverslips to eliminate the effect of the underlying mesh and to enable live-cell imaging. The results were basically similar to those obtained on the cCNF-coated meshes, i.e., (1) poor adhesion and spreading of both cell types on glass coverslips preadsorbed with FBS or BSA, (2) almost equally poor adhesion and spreading of NHDFs seeded on pure glass coverslips in a medium supplemented with FBS or BSA, but (3) relatively good adhesion and spreading of ADSCs seeded on glass coverslips in a medium with FBS or BSA (Figure S4).

These results suggest that ADSCs adhere more quickly than NHDFs; that is, mostly before the adsorption of non-cell-adhesive albumin, which is contained in FBS. This assumption was confirmed by live-cell imaging using cell trackers. Simultaneous seeding of NHDFs (red) and ADSCs (green) on a cCNF-coated glass substrate in DMEM with 10% FBS revealed that the attachment and spreading of ADSCs was quicker than the attachment of NHDFs, which were much slower in their attachment and were not able to spread properly (Supporting Video).

3.4.5. Day 3: Proliferation and Morphology of Cells on CNF-Coated Meshes. Measurements of cell metabolic activity

https://dx.doi.org/10.1021/acs.biomac.0c01097
Biomacromolecules 2020, 21, 4857−4870

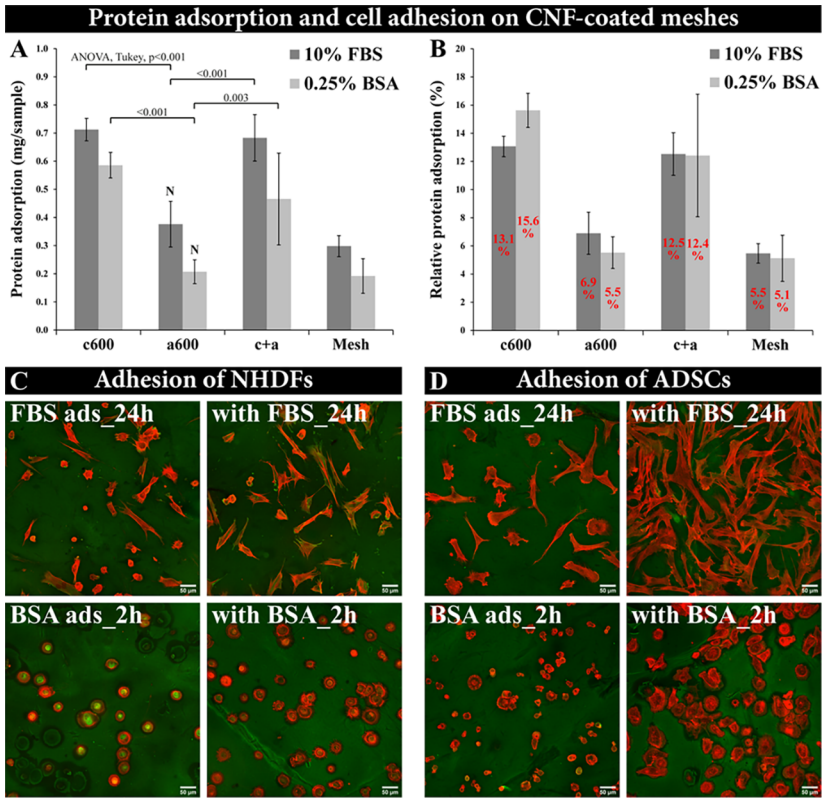

Figure 4. Adsorption of proteins on the cCNF-coated meshes measured by the Pierce BCA Protein Assay Kit (A, B), and initial adhesion of NHDFs and ADSCs on the cCNF-coated meshes with and without preadsorbed proteins (C, D). (A) Adsorption of 1.5 mL of 0.25% BSA (2.5 mg/mL) and 10% FBS (3.64 mg/mL of proteins) displayed in mg/sample. (B) Relative adsorption of 0.25% BSA (3.75 mg = 100%) and 10% FBS (5.46 mg = 100%) displayed as a percentage. Arithmetic mean ± SD from eight measurements made on four independent samples, ANOVA, Tukey's method, and statistical significance ($p \leq 0.05$). N, No significant difference compared to the noncoated mesh (mesh). Adhesion and spreading of NHDFs (C) and ADSCs (D) on cCNF-coated meshes with (FBS ads_24h and BSA ads_2h) and without (with FBS_24h and BSA_2h) preadsorbed proteins after 2 h and 24 h of cell cultivation. F-actin in the cell cytoskeleton is stained in red. Nonspecific binding of the secondary antibody on cCNF coatings and vinculin in the cells are indicated by green. A confocal microscope with an objective magnification of 20×. Scale bar = 50 μm.

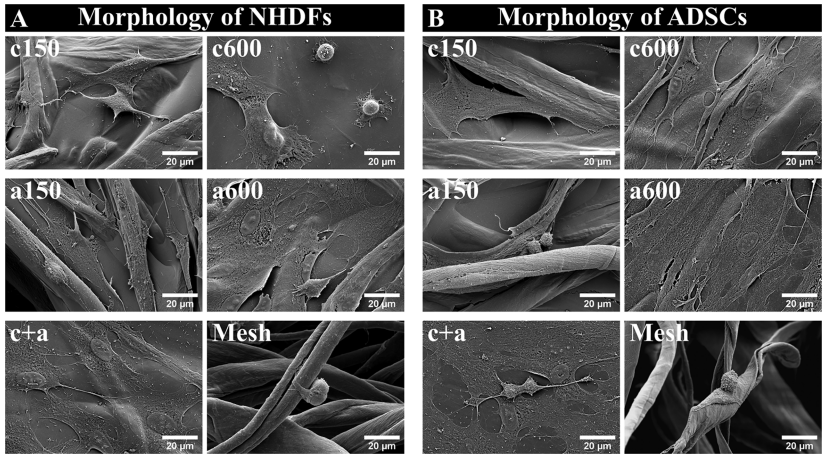

Figure 5. Morphology of NHDFs (A) and ADSCs (B) on CNF-coated and noncoated meshes on day 3 after cell seeding, acquired by SEM. Scale bar = 20 μm.

after 3 days of cultivation (Figure S5A,B) revealed that aCNF-coated meshes (a150, a600) significantly increased the proliferation capacity of both cell types compared to the noncoated meshes (mesh) and the cCNF-coated meshes (c150, c600). The metabolic activity of NHDFs on cCNF-coated meshes (c150, c600) was almost at the same level as on noncoated meshes, and it remained at almost the same level as on day 1 (cf. Figures S5A and 3A). The negative influence of cCNFs on cell behavior started to be visible also in ADSCs (Figure S3). However, the metabolic activity of the ADSCs was still slightly higher on the c150 and c600 coatings than the metabolic activity of the NHDFs (Figure S5A,B). Similarly to day 1 (Figure 3A,B), the metabolic activity of both cell types on the c+aCNF-coated meshes was comparable with the values

https://dx.doi.org/10.1021/acs.biomac.0c01097
Biomacromolecules 2020, 21, 4857−4870

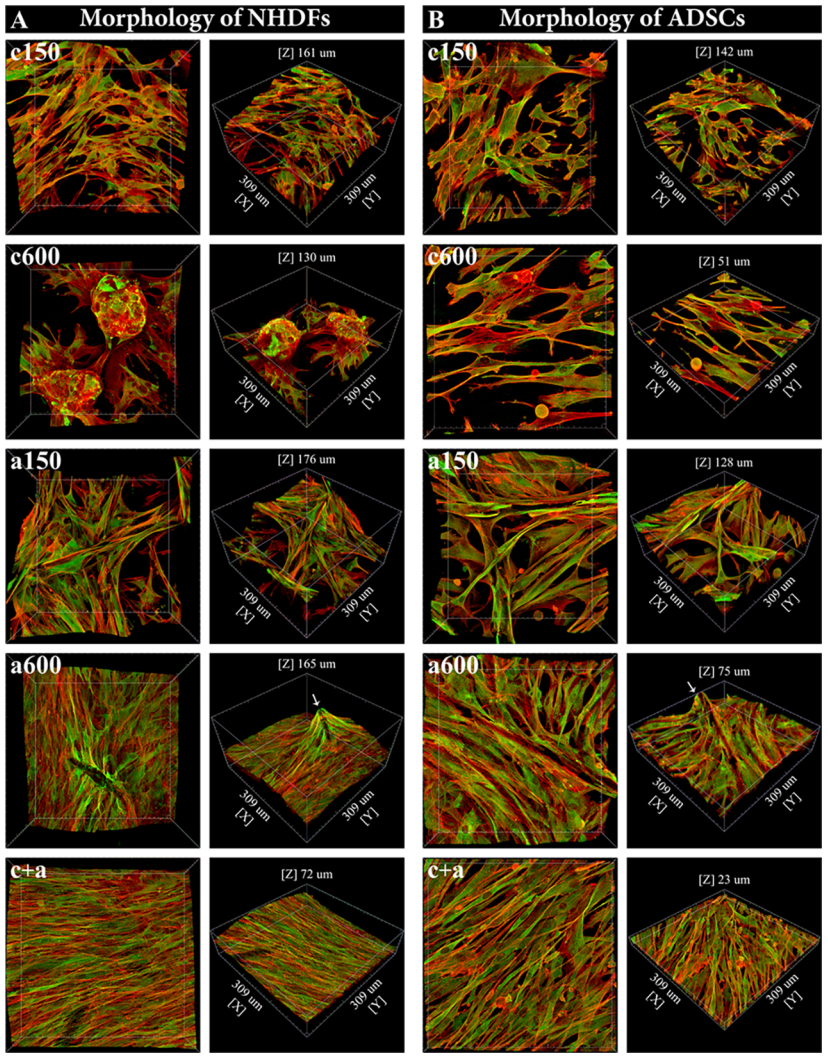

Figure 6. Morphology of NHDFs (A) and ADSCs (B), guided by the topography of the CNF-coated meshes after 7 days of cultivation. 3D projection of microscopy images (front view and side view) of the cells on CNF-coated meshes. F-actin of the cell cytoskeleton is stained in red, and vinculin in the cells is stained in green. A confocal microscope with an objective magnification of 40×.

on the control polystyrene (PS = 100%) but was significantly lower than the values on the a600 CNF-coated meshes (Figure S5A,B).

After 3 days of cultivation, the cells were mostly spread, and the morphology and the orientation of both cell types were guided by the surface topography of the CNF-coated meshes. The flat 2D surface of the c600 coatings markedly supported the growth of ADSCs (Figure 5B), while the NHDFs were poorly spread and started to detach from the c600 coatings (Figure 5A). However, this rounded morphology of the NHDFs was slightly improved by the 3D topography of the c150 coatings, where the cells acquired a more physiological spindle-like morphology (Figure 5 and S5C). Similarly, although the number of both cell types was higher on the 2D surfaces of the a600 coatings, more elongated cells were observed on the 3D surface of the a150 coatings. The cells on noncoated meshes were round and were barely attached (Figures 5 and S5C,D).

3.4.6. Day 7: Final Colonization of the CNF-Coated Meshes with Cells. The metabolic activity of ADSCs on all types of tested materials was generally lower than the metabolic activity of the NHDFs (Figure S3). However, the proliferation of both cell types on the cCNF-coated and noncoated meshes was significantly lower than that on the aCNF- and c+aCNF-coated meshes. Despite the overall low growth capacity of the cells on the cCNF coatings, the numbers of both cell types were higher on c150 than those on c600 (Figure S6A,B). On a600 and c+a, both cell types reached confluence and colonized almost the entire surface (Figure S6C,D). On day 7, the cell growth capacity on the 3D surface of a150 was equalized with the cell growth capacity on a600 and on c+a, especially in the case of NHDFs (Figure S6).

The 3D projections of microscopy images of cells on the CNF-coated meshes revealed that the 2D coatings (a600 and c+a) enhanced the proliferation and spreading of both cell types only in the *xy* directions, while the 3D coatings (a150) supported elongation of the cells on the mesh fibers and between them in all *xyz* directions (Figure 6). Therefore, the 3D surface of the a150 coatings provided more space for cell elongation and proliferation (Figures 6 and S6). The negative effect of cCNF, mainly of c600 coatings, on cell attachment was manifested by the formation of clusters of ADSCs and spheroids of NHDFs (Figures 6 and S6).

https://dx.doi.org/10.1021/acs.biomac.0c01097
Biomacromolecules 2020, 21, 4857−4870

The interaction of the cells with the material surface topography and the formation of vinculin-containing focal adhesion sites were evaluated from 3D projections of microscopy images (Figure 6). During 1 week of cultivation, the interactions between the cells and the surface topography features were established, and a positive effect of the 3D topography of the a150 coatings and also of the c150 coatings on cell growth was observed (Figures 6 and S6C,D). The cells detaching from the c600 CNF-coated meshes showed vinculin dispersed throughout the cell without creating any focal adhesions, except for the spheroidal structures, where vinculin seems to be located in the cell−cell contacts. On the c150 CNF-coated meshes, vinculin was more visible in the cells, but only a few barely detected focal adhesions were observed (Figure 6). On the aCNF-coated meshes, the cells were spread in all three dimensions and grew along the directions of the mesh fibers, and focal adhesions were clearly visible (see a150 in Figure 6). On the predominantly 2D surface of the a600 coatings, a higher vinculin signal was observed in the cells that were migrated upward to the top of the protruding aCNF-coated mesh fibers (see a600—arrows in Figure 6).

4. DISCUSSION

4.1. Properties of CNF-Based Coatings. In this study, we prepared nanocellulose-based coatings on a microfibrous cellulose mesh to improve its properties as a cell carrier in skin tissue engineering and wound healing applications.

Based on the amount of the CNF solutions that was applied, two different coating microtopographies were formed. A greater volume of the CNF solution (600 μL) resulted in the formation of a flat film-like coating on the surface of the cellulose mesh, while a lower suspension volume (150 μL) resulted in a coating that covered the individual fibers of the mesh. Although the topographies can be regulated by the volume of the solutions, the cCNF solution predominantly formed a film-like coating on the surface of the cellulose mesh, while the solution of aCNFs leaked into the mesh pores more easily and predominantly covered the individual mesh fibers (Figures 1 and S1). This behavior can be explained by the presence of larger fibrils in the cCNF solution than in the aCNF solution.[32,33] The larger cCNF fibrils were accumulated on top of the mesh fibers and prevented further penetration of the cCNF solution into the mesh pores, which resulted in a thin film on the mesh surface. This phenomenon was utilized in the preparation of the c+aCNF coatings, where the cCNF solution was first applied on the mesh followed by the application of aCNF and then by mixing of the two solutions. The larger cCNF fibrils blocked the pores and prevented penetration of the aCNFs. The aCNFs formed ionic cross-linking with the oppositely charged sidechains of the cCNFs, as the trimethylammonium ($-N(CH_3)_3^+$) group of cCNFs can form ionic bonding with carboxyl ($-COO^-$) groups of aCNFs.[34]

To describe the functionality of the CNF coating at the cell perception level, the surface roughness of the CNF coating was measured. The roughnesses of the c600 ($R_a \sim 9.04$ nm) and a600 ($R_a \sim 10.2$ nm) 2D coatings were similar (Figures 1 and S1). The greater variation in the roughness of c600 is probably due to the locally distributed larger fibers present in the cCNF solution.[12,33] The greater roughness of c+a ($R_a \sim 55.76$ nm) could be due to strong ionic cross-linking between the anionic $-COO^-$ and cationic $-N(CH_3)_3^+$ groups that probably formed the local aggregation of the nanofibrils.

The different surface chemistries of the CNF coatings influence the wettability and the water uptake, which results in the different swelling properties and the different softening dynamics of the coatings. The more hydrophilic surface of aCNFs presents $-COO^-$ and hydroxyl ($-OH$) functional groups that enable hydrogen bonding.[23] Thus, the aCNF coating binds more water on the surface, resulting in a lower contact angle (31°) with water than that on the surface of the cCNFs, which contains not only hydrophilic $-OH$ groups but also more hydrophobic methyl ($-CH_3$) groups. The $-CH_3$ groups do not form hydrogen bonds.[23] This renders the cCNF surface more hydrophobic, resulting in a higher contact angle on cCNFs (65°) with water. The hydrogen-bonding capacity may also influence the penetration of the fibrils into the mesh pores, as discussed above. The cellulose mesh has more hydrogen-bonding sites for $-COO^-$ and $-OH$ groups of aCNFs than those for the $-CH_3$ of the cCNFs.[23] HPTMA functionalization of the $-OH$ group in C2 of the cCNF cellulose backbone[23,35] resulted in a larger functionalized moiety than that in the case of the smaller COO^--functionalized $-OH$ group in C6 of aCNFs. Thus, the cCNFs form a more branched and spongier structure (see the structures in Chaker and Boufi[23]), which enables cCNFs to take up more water[36] than aCNFs. The positively charged $-N(CH_3)_3^+$ groups interact with dipolar substituents,[37] enabling solvation even though the $-CH_3$ groups make the cCNFs more hydrophobic.

The swelling ratio and the changes in surface stiffness were measured with time. The surface stiffness of all wetted CNF coatings was dramatically reduced in comparison with the coatings in a dry state. The greater stiffness of the aCNF coatings in comparison with that of the cCNF coatings at the beginning can be explained by the capacity of oxidized nanofibrils to build up a strong network held together by hydrogen bonding,[23] while the presence of the 2-HPTMA chloride moiety of the cCNFs reduces hydrogen bonding and thus weakens the cohesion of the network.[23] The softening of aCNFs with time could also be due to displacement of the hydrogen bonding between the $-COO^-$ and $-OH$ groups by the hydrogen bonding between the $-COO^-$ and H_2O molecules. In addition, the charged groups of CNFs should also increase the hydrophilicity of the material. It has been reported that TEMPO oxidation increases the negative charge, resulting in electrostatic repulsion between the fibrils in a wet state; thus, the high negative charge of TEMPO-oxidized CNFs causes low water resistance[38] and high swelling.[28] The surface charges of our aCNF and cCNF coatings are probably similar to the reported ζ-potential values for the corresponding grades of CNFs, which were −69.5 mV (for aCNFs) and +41 mV (for cCNFs).[33,39] The negative surface charge, in combination with hydrogen bonding to the water molecules, could explain the swelling and softening of aCNF coatings over time, while the branched sponge-like structure of $-N(CH_3)_3^+$ groups could contribute to the higher total water uptake of cCNF coatings. The swelling of cCNFs decreased slightly, while the mean stiffness increased slightly. This is particularly apparent during the immersion of cCNFs in DMEM. The ions present in DMEM may enable ionic cross-linking to some extent, which reduces the water uptake and increases the strength of the material, which was observed for cCNFs over time. In summary, the general trend in stiffness follows the general trend of the swelling of the coatings. There was a significant difference in swelling of c600 between water and

https://dx.doi.org/10.1021/acs.biomac.0c01097
Biomacromolecules 2020, 21, 4857−4870

DMEM (Figure 2A). Unlike the deionized water used in our experiments, DMEM contains a variety of ions that can interact with the positively charged moieties of c600, and subsequently, fewer water molecules are occupied around these sites, resulting in less water uptake than that in the case of the samples soaked in deionized water (Figure 2A).

The microtopographical structure of the c+a combination is similar to that of the cCNFs, while the contact angle, swelling, and stiffness properties more closely resemble those measured on the aCNF coatings. The roughness of the c+aCNF coating differs from the roughness of both cCNFs and aCNFs. The values of contact angle and the swelling of c+aCNFs are closer to the values of aCNFs than to the values of cCNFs. This is probably due to strong ionic cross-linking between c+aCNFs, which prevents the water from penetrating into the structure. However, the c+aCNF coating contains more hydrophilic hydrogen-bonding groups than the cCNF coatings, which may also have an effect on the swelling and stiffness. The stiffness of the c+aCNFs coating did not decrease over time, as was observed with the aCNF coatings. This can be explained by strong ionic cross-linking, which can reduce the interactions of hydrogen-bonding groups with water molecules. The c+aCNF combination, therefore, offers an interesting set of properties, which might be further adjusted to create not only film-like coatings for cell cultivation but also 3D cross-linked CNF gels for cell embedding and for 3D printing.

4.2. Cell Behavior Influenced by the Properties of CNF Coatings. A comparison was made between two coating microtopographies—the 2D film-like topography and the 3D coating topography—for differences in cell−material interactions. Our results suggest that the flat substrates of c600, a600, and c+a, where the cells formed monolayers, can be suitable for cell sheet technology. This technology enables the creation of self-standing, mechanically resistant, continuous cell sheets that can be replanted on other substrates, such as tissue-engineered skin constructs *in vitro* or wound beds *in vivo*. The cell sheets can be released from cellulose substrates by cellulase enzymes, which are not cytotoxic. In addition, unlike proteolytic enzymes such as trypsin or collagenase, they preserve the cell-to-cell connections and the ECM proteins within the sheets.[40] The 3D substrates of c150 and a150, where the cells penetrated into the material, are also promising for tissue engineering and for future clinical applications. 3D substrates made of a CNF-coated cellulose mesh might provide sufficient space for the cells for *in vitro* long-term cell cultivation and might allow for better diffusion of nutrients than the widely used hydrogels.[41]

Not only the microtopography of the material but also the cell−material interactions can also be modulated by the elasticity, roughness, and surface chemistry of the material. The elasticity of natural tissues varies from 0.2 to 1 kPa for soft tissues, such as brain or fat, via medium-soft tissues such as skin (10−30 kPa), to hard tissues of more than 10^5 kPa, e.g., for bone.[42,43] The stiffness of our CNF coatings is close to the stiffness of native tissues such as fibrotic tissue (100 kPa), cartilage, and tendon (approaching 10^3 kPa).[25,42] By comparison, Kummala et al. introduced 0.1 mm thick CNF films with Young's modulus between 1 and 60 kPa.[3] Although the CNF substrates used in this study were much softer than the conventional cell culture substrates (GPa),[42] they can be considered as relatively stiff substrates at the cell perception level. For example, Achterberg et al. determined Young's modulus of native human dermis using AFM between 0.1 and 10 kPa, depending on the location, which is at least 10 times softer than our CNF substrates.[44]

Not only the stiffness but also the roughness is important at the cell perception level, especially for initial cell attachment, because the cell focal adhesions are in the nanoscale range from 2 to 200 nm.[45] Alterations in material surface roughness can influence the adhesion and further proliferation of fibroblasts, as described by Bourkoula et al., and also the spreading and differentiation of mesenchymal stem cells, as observed by Hou et al.[46,47] While the aCNF and cCNF coatings showed relatively low roughness, the c+aCNF combination showed a rougher surface (see $R_a \sim 55.76$ nm in Figure 1), which corresponds to the least rough surface measured by Hou et al.[47] These authors revealed that the substrates with the lowest studied roughness ($R_a \sim 31.49$ nm) supported cell adhesion and spreading, but the cell−substrate tension and osteogenesis were only moderate in comparison with the substrates with intermediate roughness ($R_a \sim 183.16$ nm).[47]

Although the studied CNF surfaces differ in many parameters, including the microtopography, roughness, swelling ratio, and Young's modulus, we assume that the main cell adhesion-modulating factor is the surface chemistry of CNFs, which governs the surface charge and wettability. The surface chemistry can determine the composition of proteins adsorbed on CNF surfaces and the speed with which various serum proteins are adsorbed and the cells are adhered.[24] It is generally known that cells adhere to material substrates through the proteins adsorbed to the material surface from the biological fluids. Adhesion-mediating proteins, such as fibronectin, vitronectin, collagen, and laminin, contain specific amino acid sequences (e.g., RGD) that can be recognized by integrin receptors on cells, while albumin is nonadhesive for cells due to the lack of these specific adhesion sequences in its molecule. However, albumin can improve the geometric conformation of the cell adhesion-mediating proteins for binding by cell adhesion receptors.[21] Based on the Vroman effect—i.e., the dynamics with which proteins adsorb and interchange in time—we can assume that the NHDFs and ADSCs adhered to a layer of proteins that differ in their composition.[48]

We have demonstrated that cCNFs with positively charged $-N(CH_3)_3^+$ tails adsorb more proteins, predominantly BSA, than aCNFs with negatively charged −COO functional groups (Figure 4). Similar results were achieved by Attwood et al.[50] with well-defined positively charged $-N(CH_3)_3^+$- and $-COO^-$-terminated self-assembled monolayers (SAMs) and also by Courtenay et al., who quantified the proteins adsorbed from FBS, specifically BSA, on positively charged GTMAC-modified cCNF scaffolds.[49,50] They revealed increasing protein adsorption with increased cationization. The greater affinity of BSA to positively charged surfaces could be due to the negative character of the BSA at the physiological pH of DMEM.[51,52] We could expect that the negatively charged proteins in FBS, such as fibronectin, vitronectin, and BSA, have the same electrostatic affinity to the positively charged surfaces at the physiological pH of DMEM due to their similar theoretical isoelectric points.[26] However, the concentration of BSA at a level between 35 and 50 mg/mL in FBS is 100−1000 times higher than the concentration of other proteins,[26,27] which makes BSA the most abundant adsorbed protein on positively charged substrates. Furthermore, Hoshiba et al.[26] revealed that the absolute amount of adsorbed proteins on chemically

https://dx.doi.org/10.1021/acs.biomac.0c01097
Biomacromolecules 2020, 21, 4857−4870

modified charged methacrylates (MA) is less important than the protein composition of the most superficial layer. In their study, positively charged $-N(CH_3)_2^+$-terminated MA adsorbed more proteins from FBS than were absorbed by negatively charged $-COO^-$-terminated MA. However, the most superficial layer of $-COO^-$-terminated MA contained more cell adhesion-mediating proteins, mainly vitronectin, and also fibronectin in its more suitable conformation for cell adhesion.[26] In general, the positive effect of negatively charged $-COO^-$ termination on cell adhesion, spreading, and proliferation of various substrates has been confirmed by many other research groups.[6,26,53]

The abundant yields of BSA on the surface of the cCNF-coated meshes probably reduced the amount of attached NHDFs, but it did not influence the attachment of the ADSCs. Based on Courtenay et al.'s work, we hypothesize that the ADSCs were attracted by the positive charge on the surface of the cCNFs, and their attachment can be classified as protein-independent electrostatically mediated adhesion.[6,8] Unlike Courtenay et al., we observed this phenomenon with ADSCs not only in a serum-free medium but also in a serum-containing medium (Figure S4 and the Supporting Video).[8] This could be due to a higher adhesion speed of ADSCs than that of NHDFs, which enabled them to adhere before the adsorption of BSA took place. This was clearly visible especially on the ADSCs that were not able to adhere to the cCNF coatings, which were preadsorbed with FBS or nonadhesive BSA (Figure 4). Although ADSCs adhered to the cCNF coatings in large numbers, their cell adhesion forces were rather weak, as was manifested by the suppression of proliferation and by the formation of clusters and spheroids. Courtenay et al. reported similar findings, revealing that there was greater cell adhesion on cationic nanocellulose than on anionic nanocellulose in the serum-free medium, while the cells in the serum-containing medium responded in the opposite way.[6] This confirms that the cells in a serum-free medium adhered to positively charged substrates via integrin-independent electrostatic interactions, while cell adhesion was suppressed in the serum-containing medium by the adsorption of the proteins in an inappropriate spectrum and conformation. Negatively charged substrates therefore seem to be more suitable for cells due to the presence of stronger protein-mediated integrin-dependent adhesions and also weak electrostatic cell−material interactions.[26,53] In addition, this specific integrin-mediated cell adhesion is capable of delivering appropriate signals to cells, ensuring the viability, proliferation, and other functions of the cells.

The adsorption of proteins and further cell adhesion is also mediated by the hydrophilicity or hydrophobicity of the surfaces.[27,50,53] Although both CNF coatings were expected to be hydrophilic due to the charged $-COO^-$ and $-N(CH_3)_3^+$ functional groups,[50] the cCNFs (contact angle 65°) were more hydrophobic than the aCNFs (contact angle 31°). The presence of neutral $-CH_3$ groups on the surface of cCNFs probably reduced the hydrophilicity, which made the surface less attractive than the surface of aCNFs for the cells in a serum-containing medium. Similar results were achieved by McClary et al. and Faucheux et al. with $-CH_3$- and $-COO^-$-terminated SAMs.[53,54] In addition, Arima and Iwata[27] described how moderately hydrophilic SAMs enhanced cell adhesion even though they were preadsorbed with BSA, while hydrophobic SAMs preadsorbed with BSA inhibited cell adhesion. This was due to the strongly adsorbed BSA on hydrophobic SAMs, which cannot be replaced by cell adhesion-mediating proteins as effectively as on hydrophilic SAMs, where the proteins interchanged due to the Vroman effect.[27,48] We could assume that both aCNFs and c+aCNFs were suitable for cell adhesion and growth due to their hydrophilic surface character. Although the level of adsorbed BSA on c+aCNFs was comparable to the level of less hydrophilic cCNFs (Figure 4), the hydrophilic surface character of c+aCNFs probably enabled BSA to be replaced by the cell adhesion-mediating proteins in the most superficial layer of the adsorbed proteins. However, the less adhesive cCNF coatings for cells can also occupy an important place in tissue engineering. As indicated by Figures 6 and S6, these surfaces can be used for generating three-dimensional multicellular spheroids, similar to the albumin-coated surfaces in a study by Okuyama et al.[55]

5. CONCLUSIONS AND FURTHER PERSPECTIVES

In this study, we have developed novel electroactive coatings on a cellulose mesh based on cationic nanofibrils (cCNFs) or based on anionic cellulose nanofibrils (aCNFs) or based on a 1:1 mixture of both types of nanofibrils (c+aCNFs). When seeded with normal human dermal fibroblasts (NHDFs) or human adipose-tissue-derived stem cells (ADSCs), the negatively charged aCNFs, and also the mixture of c+aCNFs, appeared to provide better substrates for cell adhesion and growth than the positively charged cCNFs. This was demonstrated mainly with NHDFs. The most likely explanation for this finding is that the positively charged cCNFs were more hydrophobic and they preferentially adsorbed albumin, which is nonadhesive for cells. However, negatively charged aCNFs and combined c+aCNFs were hydrophilic, and they adsorbed more serum proteins mediating cell adhesion, such as vitronectin and fibronectin. In addition, cCNFs attracted the cells via electrostatic forces, and this non-integrin-mediated cell adhesion is less efficient in maintaining the viability and the growth activity of cells. Nevertheless, all three types of CNF coatings can be utilized in specific biomedical applications, e.g., in skin tissue replacement, using cell sheet technology in the case of aCNFs and c+aCNFs, and the generation of cell spheroids, in the case of cCNFs. In addition, c+aCNFs provide an interesting combination of the properties of cCNFs and aCNFs: the microtopographical structure is similar to that of cCNFs, while the contact angle, swelling, and stiffness properties more closely resemble the values for aCNF coatings. In the future, the properties of the c+aCNF combination can be further adjusted to create not only film-like coatings for cell cultivation but also 3D cross-linked CNF gels for cell embedding and 3D printing.

■ ASSOCIATED CONTENT

Supporting Information

The Supporting Information is available free of charge at https://pubs.acs.org/doi/10.1021/acs.biomac.0c01097.

Supporting methods and figures (PDF)

Adhesion and spreading of NHDFs (red tracker) and ADSCs (green tracker) in coculture on cCNF-coated glass (phase contrast) during the first 22 h after cell seeding (Supporting Video) (AVI)

https://dx.doi.org/10.1021/acs.biomac.0c01097
Biomacromolecules 2020, 21, 4857−4870

AUTHOR INFORMATION

Corresponding Authors

Julia Pajorova − *Department of Biomaterials and Tissue Engineering, Institute of Physiology of the Czech Academy of Sciences, 14220 Prague, Czech Republic; 2nd Faculty of Medicine, Charles University, 15006 Prague, Czech Republic;* orcid.org/0000-0001-5545-0031; Email: Julia.Pajorova@fgu.cas.cz

Anne Skogberg − *BioMediTech Institute and Faculty of Medicine and Health Technology (MET), Tampere University, 33720 Tampere, Finland*; Email: Anne.Skogberg@tuni.fi

Lucie Bacakova − *Department of Biomaterials and Tissue Engineering, Institute of Physiology of the Czech Academy of Sciences, 14220 Prague, Czech Republic*; Email: Lucie.Bacakova@fgu.cas.cz

Pasi Kallio − *BioMediTech Institute and Faculty of Medicine and Health Technology (MET), Tampere University, 33720 Tampere, Finland;* orcid.org/0000-0001-6698-774X; Email: Pasi.Kallio@tuni.fi

Authors

Daniel Hadraba − *Department of Biomathematics, Institute of Physiology of the Czech Academy of Sciences, 14220 Prague, Czech Republic*

Antonin Broz − *Department of Biomaterials and Tissue Engineering, Institute of Physiology of the Czech Academy of Sciences, 14220 Prague, Czech Republic*

Martina Travnickova − *Department of Biomaterials and Tissue Engineering, Institute of Physiology of the Czech Academy of Sciences, 14220 Prague, Czech Republic; 2nd Faculty of Medicine, Charles University, 15006 Prague, Czech Republic*

Marketa Zikmundova − *Department of Biomaterials and Tissue Engineering, Institute of Physiology of the Czech Academy of Sciences, 14220 Prague, Czech Republic*

Mari Honkanen − *Tampere Microscopy Center, Tampere University, 33720 Tampere, Finland*

Markus Hannula − *BioMediTech Institute and Faculty of Medicine and Health Technology (MET), Tampere University, 33720 Tampere, Finland*

Panu Lahtinen − *VTT Technical Research Center of Finland, 02150 Espoo, Finland*

Maria Tomkova − *Faculty of Biotechnology and Food Sciences, Slovak University of Agriculture in Nitra, 94976 Nitra, Slovak Republic*

Complete contact information is available at: https://pubs.acs.org/10.1021/acs.biomac.0c01097

Author Contributions

[#]J.P. and A.S. contributed equally to this work. The manuscript was written through the contribution of all authors. All authors have approved the final version of the manuscript. J.P. and A.S. planned, performed, and analyzed the experimental work, with the exception of the microCT imaging and analysis (M. Hannula) and the AFM scanning and analysis (D.H.). A.B., M.Z., and M. Tomkova helped with the cell experiments and microscopy imaging. M. Travnickova and J.P. performed the ADSC isolations. M. Honkanen performed SEM scanning. P.L. contributed to the CNF preparation. P.K. and L.B. contributed to the conception of the study, coordination of the work, and structuring and editing the manuscript.

Funding

This study was supported by the Grant Agency of Czech Republic (Grant no. 20-01641S), by the Grant Agency of Charles University in Prague (Grant no. 756218), by the Academy of Finland through the WoodBone Project (Grant no. 326399), by the Centre of Excellence in Body-on-Chip Research (Grant no. 336785), and by the Ministry of Education, Youth and Sports of the Czech Republic (MEYS CR) within LQ1604 National Sustainability Program II (BIOCEV-FAR Project). Julia Pajorova received funding (Development of HR capabilities, internationalization, popularization and IP utilization, No. CZ.02.2.69/0.0/0.0/16_028/0006226) for traveling to Finland.

Notes

The authors declare no competing financial interest.

ACKNOWLEDGMENTS

We acknowledge the Light Microscopy Core Facility, IMG ASCR, Prague, Czech Republic, supported by MEYS CR (LM2015062, CZ.02.1.01/0.0/0.0/16_013/0001775), OPPK (CZ.2.16/3.1.00/21547), and MEYS CR (LO1419), for its support with confocal imaging and image analysis presented here. We further acknowledge the IPHYS imaging facility supported by MEYS CR (LM2018129) and CF Nanobiotechnology, Jan Pribyl, supported by MEYS CR (LM2018127). Dr. M. Tomkova acknowledges the International Visegrad Fund (No. 51910646). Ing. Tomas Sopuch, from Holzbecher, spol. s.r.o., is acknowledged for providing the cellulose mesh. Dr. Ivan Kostic and Dr. Milan Beno, from the Slovak Academy of Sciences, are acknowledged for their help with sample preparation and with preliminary imaging on the scanning electron microscope. SEM studies were carried out at Tampere University using facilities provided by the Tampere Microscopy Center. James Morrison, Academic Editor (James-Edits Academic Editing, Nelson, Marlborough & Tasman, New Zealand), and Robin Healey (Czech Technical University in Prague, Czech Republic) are gratefully acknowledged for their language revision of the manuscript. We also acknowledge Mari Leino (Senior Research Technician, VTT) for TEMPO oxidation of CNFs and Pia Willberg-Keyriläinen (Senior Scientist, VTT) for cationization of CNFs.

REFERENCES

(1) Nechyporchuk, O.; Belgacem, M. N.; Bras, J. Production of cellulose nanofibrils: A review of recent advances. *Ind. Crops Prod.* **2016**, *93*, 2−25.

(2) Zhang, Y. X.; Nypelo, T.; Salas, C.; Arboleda, J.; Hoeger, I. C.; Rojas, O. J. Cellulose Nanofibrils: From Strong Materials to Bioactive Surfaces. *J. Renewable Mater.* **2013**, *1*, 195−211.

(3) Kummala, R.; Xu, W. Y.; Xu, C. L.; Toivakka, M. Stiffness and swelling characteristics of nanocellulose films in cell culture media. *Cellulose* **2018**, *25*, 4969−4978.

(4) Dufresne, A. Nanocellulose: a new ageless bionanomaterial. *Mater. Today* **2013**, *16*, 220−227.

(5) Ling, S.; Chen, W.; Fan, Y.; Zheng, K.; Jin, K.; Yu, H.; Buehler, M. J.; Kaplan, D. L. Biopolymer nanofibrils: structure, modeling, preparation, and applications. *Prog. Polym. Sci.* **2018**, *85*, 1−56.

(6) Courtenay, J. C.; Johns, M. A.; Galembeck, F.; Deneke, C.; Lanzoni, E. M.; Costa, C. A.; Scott, J. L.; Sharma, R. I. Surface modified cellulose scaffolds for tissue engineering. *Cellulose* **2017**, *24*, 253−267.

(7) Weishaupt, R.; Siqueira, G.; Schubert, M.; Tingaut, P.; Maniura-Weber, K.; Zimmermann, T.; Thony-Meyer, L.; Faccio, G.; Ihssen, J. TEMPO-Oxidized Nanofibrillated Cellulose as a High Density

Carrier for Bioactive Molecules. *Biomacromolecules* **2015**, *16*, 3640−3650.
(8) Courtenay, J. C.; Deneke, C.; Lanzoni, E. M.; Costa, C. A.; Bae, Y.; Scott, J. L.; Sharma, R. I. Modulating cell response on cellulose surfaces; tunable attachment and scaffold mechanics. *Cellulose* **2018**, *25*, 925−940.
(9) Kummala, R.; Veliz, D. S.; Fang, Z. Q.; Xu, W. Y.; Abitbol, T.; Xu, C. L.; Toivakka, M. Human Dermal Fibroblast Viability and Adhesion on Cellulose Nanomaterial Coatings: Influence of Surface Characteristics. *Biomacromolecules* **2020**, *21*, 1560−1567.
(10) Hua, K.; Carlsson, D. O.; Alander, E.; Lindstrom, T.; Stromme, M.; Mihranyan, A.; Ferraz, N. Translational study between structure and biological response of nanocellulose from wood and green algae. *RSC Adv.* **2014**, *4*, 2892−2903.
(11) Rashad, A.; Mustafa, K.; Heggset, E. B.; Syverud, K. Cytocompatibility of Wood-Derived Cellulose Nanofibril Hydrogels with Different Surface Chemistry. *Biomacromolecules* **2017**, *18*, 1238−1248.
(12) Skogberg, A.; Maki, A. J.; Mettanen, M.; Lahtinen, P.; Kallio, P. Cellulose Nanofiber Alignment Using Evaporation-Induced Droplet-Casting, and Cell Alignment on Aligned Nanocellulose Surfaces. *Biomacromolecules* **2017**, *18*, 3936−3953.
(13) Xiong, G. Y.; Luo, H. L.; Zhang, C.; Zhu, Y.; Wan, Y. Z. Enhanced biological behavior of bacterial cellulose scaffold by creation of macropores and surface immobilization of collagen. *Macromol. Res.* **2015**, *23*, 734−740.
(14) Lou, Y. R.; Kanninen, L.; Kuisma, T.; Niklander, J.; Noon, L. A.; Burks, D.; Urtti, A.; Yliperttula, M. The Use of Nanofibrillar Cellulose Hydrogel As a Flexible Three-Dimensional Model to Culture Human Pluripotent Stem Cells. *Stem Cells Dev.* **2014**, *23*, 380−392.
(15) Xu, W. Y.; Zhang, X.; Yang, P. R.; Langvik, O.; Wang, X. J.; Zhang, Y. C.; Cheng, F.; Osterberg, M.; Willfor, S.; Xu, C. L. Surface Engineered Biomimetic Inks Based on UV Cross-Linkable Wood Biopolymers for 3D Printing. *ACS Appl. Mater. Interfaces* **2019**, *11*, 12389−12400.
(16) Koivuniemi, R.; Hakkarainen, T.; Kiiskinen, J.; Kosonen, M.; Vuola, J.; Valtonen, J.; Luukko, K.; Kavola, H.; Yliperttula, M. Clinical Study of Nanofibrillar Cellulose Hydrogel Dressing for Skin Graft Donor Site Treatment. *Adv. Wound Care* **2020**, *9*, 199−210.
(17) Kiiskinen, J.; Merivaara, A.; Hakkarainen, T.; Kaariainen, M.; Miettinen, S.; Yliperttula, M.; Koivuniemi, R. Nanofibrillar cellulose wound dressing supports the growth and characteristics of human mesenchymal stem/stromal cells without cell adhesion coatings. *Stem Cell Res. Ther.* **2019**, *10*, 1−13.
(18) Bacakova, L.; Pajorova, J.; Bacakova, M.; Skogberg, A.; Kallio, P.; Kolarova, K.; Svorcik, V. Versatile Application of Nanocellulose: From Industry to Skin Tissue Engineering and Wound Healing. *Nanomaterials* **2019**, *9*, 1−39.
(19) Isogai, A.; Saito, T.; Fukuzumi, H. TEMPO-oxidized cellulose nanofibers. *Nanoscale* **2011**, *3*, 71−85.
(20) Voisin, H.; Bergstrom, L.; Liu, P.; Mathew, A. P. Nanocellulose-Based Materials for Water Purification. *Nanomaterials* **2017**, *7*, 1−19.
(21) Bacakova, L.; Filova, E.; Parizek, M.; Ruml, T.; Svorcik, V. Modulation of cell adhesion, proliferation and differentiation on materials designed for body implants. *Biotechnol. Adv.* **2011**, *29*, 739−767.
(22) Jackson, J. K.; Letchford, K.; Wasserman, B. Z.; Ye, L.; Hamad, W. Y.; Burt, H. M. The use of nanocrystalline cellulose for the binding and controlled release of drugs. *Int. J. Nanomed.* **2011**, *6*, 321−330.
(23) Chaker, A.; Boufi, S. Cationic nanofibrillar cellulose with high antibacterial properties. *Carbohyd. Polym.* **2015**, *131*, 224−232.
(24) Syverud, K. Tissue Engineering Using Plant-Derived Cellulose Nanofibrils (CNF) as Scaffold Material. *ACS Symp. Ser.* **2017**, *1251*, 171−189.
(25) Discher, D. E.; Janmey, P.; Wang, Y. L. Tissue cells feel and respond to the stiffness of their substrate. *Science* **2005**, *310*, 1139−1143.
(26) Hoshiba, T.; Yoshikawa, C.; Sakakibara, K. Characterization of Initial Cell Adhesion on Charged Polymer Substrates in Serum-Containing and Serum-Free Media. *Langmuir* **2018**, *34*, 4043−4051.
(27) Arima, Y.; Iwata, H. Effect of wettability and surface functional groups on protein adsorption and cell adhesion using well-defined mixed self-assembled monolayers. *Biomaterials* **2007**, *28*, 3074−3082.
(28) Saito, T.; Nishiyama, Y.; Putaux, J. L.; Vignon, M.; Isogai, A. Homogeneous suspensions of individualized microfibrils from TEMPO-catalyzed oxidation of native cellulose. *Biomacromolecules* **2006**, *7*, 1687−1691.
(29) Estes, B. T.; Diekman, B. O.; Gimble, J. M.; Guilak, F. Isolation of adipose-derived stem cells and their induction to a chondrogenic phenotype. *Nat. Protoc.* **2010**, *5*, 1294−1311.
(30) Bacakova, L.; Zarubova, J.; Travnickova, M.; Musilkova, J.; Pajorova, J.; Slepicka, P.; Kasalkova, N. S.; Svorcik, V.; Kolska, Z.; Motarjemi, H.; Molitor, M. Stem cells: their source, potency and use in regenerative therapies with focus on adipose-derived stem cells - a review. *Biotechnol. Adv.* **2018**, *36*, 1111−1126.
(31) Travnickova, M.; Pajorova, J.; Zarubova, J.; Krocilova, N.; Molitor, M.; Bacakova, L. The Influence of Negative Pressure and of the Harvesting Site on the Characteristics of Human Adipose Tissue-Derived Stromal Cells from Lipoaspirates. *Stem Cells Int.* **2020**, *2020*, No. 1016231.
(32) Lahtinen, P.; Liukkonen, S.; Pere, J.; Sneck, A.; Kangas, H. A Comparative Study of Fibrillated Fibers from Different Mechanical and Chemical Pulps. *BioResources* **2014**, *9*, 2115−2127.
(33) Pöhler, T.; Lappalainen, T.; Tammelin, T.; Eronen, P.; Hiekkataipale, P.; Vehniäinen, A.; Koskinen, T. M. In Influence of fibrillation method on the character of nanofibrillated cellulose (NFC). International Conference on Nanotechnology for the Forest Products Industry. TAPPI Press: Espoo, Finland, 2010; pp 437−458.
(34) Montazer, M.; Harifi, T. In 5 - Nanosurface Activation. *Nanofinishing of Textile Materials*; Montazer, M.; Harifi, T., Eds.; Woodhead Publishing, 2018; pp 65−82.
(35) Pahimanolis, N.; Salminen, A.; Penttila, P. A.; Korhonen, J. T.; Johansson, L. S.; Ruokolainen, J.; Serimaa, R.; Seppala, J. Nanofibrillated cellulose/carboxymethyl cellulose composite with improved wet strength. *Cellulose* **2013**, *20*, 1459−1468.
(36) Zhang, K.; Barhoum, A.; Xiaoqing, C.; Li, H.; Samyn, P. In Cellulose Nanofibers: Fabrication and Surface Functionalization Techniques. *Handbook of Nanofibers*; Barhoum, A.; Bechelany, M.; Makhlouf, A. S. H., Eds.; Springer International Publishing: Cham, 2019; pp 409−449.
(37) Headley, A. D.; Mcmurry, M. E. The Influence of Solvents on the Basicity of Dipolar Amines. *J. Phys. Org. Chem.* **1994**, *7*, 63−67.
(38) Orelma, H.; Filpponen, I.; Johansson, L. S.; Osterberg, M.; Rojas, O. J.; Laine, J. Surface Functionalized Nanofibrillar Cellulose (NFC) Film as a Platform for Immunoassays and Diagnostics. *Biointerphases* **2012**, *7*, 1−12.
(39) Sneck, A.; Atsushi, T.; Meyer, V.; Kreztzschmar, J. In Advanced characterization techniques to evaluate the structure of nanofibrillated cellulose, SUNPAP Project − Final Conference, Milan, Italy, 2012.
(40) Sakai, S.; Ito, S.; Ogushi, Y.; Hashimoto, I.; Hosoda, N.; Sawae, Y.; Kawakami, K. Enzymatically fabricated and degradable microcapsules for production of multicellular spheroids with well-defined diameters of less than 150 mu m. *Biomaterials* **2009**, *30*, 5937−5942.
(41) Duval, K.; Grover, H.; Han, L. H.; Mou, Y.; Pegoraro, A. F.; Fredberg, J.; Chen, Z. Modeling Physiological Events in 2D vs. 3D Cell Culture. *Physiology* **2017**, *32*, 266−277.
(42) Skardal, A.; Mack, D.; Atala, A.; Soker, S. Substrate elasticity controls cell proliferation, surface marker expression and motile phenotype in amniotic fluid-derived stem cells. *J. Mech. Behav. Biomed. Mater.* **2013**, *17*, 307−316.
(43) Yang, Y. J.; Wang, L. Y.; Yan, F.; Xiang, X.; Tang, Y. J.; Zhang, L. Y.; Liu, J. B.; Qiu, L. Determination of Normal Skin Elasticity by Using Real-time Shear Wave Elastography. *J. Ultrasound Med.* **2018**, *37*, 2507−2516.
(44) Achterberg, V. F.; Buscemi, L.; Diekmann, H.; Smith-Clerc, J.; Schwengler, H.; Meister, J. J.; Wenck, H.; Gallinat, S.; Hinz, B. The

https://dx.doi.org/10.1021/acs.biomac.0c01097
Biomacromolecules 2020, 21, 4857−4870

Nano-Scale Mechanical Properties of the Extracellular Matrix Regulate Dermal Fibroblast Function. *J. Invest. Dermatol.* **2014**, *134*, 1862−1872.
(45) Kim, D. H.; Provenzano, P. P.; Smith, C. L.; Levchenko, A. Matrix nanotopography as a regulator of cell function. *J. Cell Biol.* **2012**, *197*, 351−360.
(46) Bourkoula, A.; Constantoudis, V.; Kontziampasis, D.; Petrou, P. S.; Kakabakos, S. E.; Tserepi, A.; Gogolides, E. Roughness threshold for cell attachment and proliferation on plasma micro-nanotextured polymeric surfaces: the case of primary human skin fibroblasts and mouse immortalized 3T3 fibroblasts. *J. Phys. D: Appl. Phys.* **2016**, *49*, No. 304002.
(47) Hou, Y.; Xie, W. Y.; Yu, L. X.; Camacho, L. C.; Nie, C. X.; Zhang, M.; Haag, R.; Wei, Q. Surface Roughness Gradients Reveal Topography-Specific Mechanosensitive Responses in Human Mesenchymal Stem Cells. *Small* **2020**, *16*, No. 1905422.
(48) Vroman, L.; Adams, A. L.; Fischer, G. C.; Munoz, P. C. Interaction of High Molecular-Weight Kininogen, Factor-Xii, and Fibrinogen in Plasma at Interfaces. *Blood* **1980**, *55*, 156−159.
(49) Courtenay, J. C.; Filgueiras, J. G.; deAzevedo, E. R.; Jin, Y.; Edler, K. J.; Sharma, R. I.; Scott, J. L. Mechanically robust cationic cellulose nanofibril 3D scaffolds with tuneable biomimetic porosity for cell culture. *J. Mater. Chem. B* **2019**, *7*, 53−64.
(50) Attwood, S. J.; Kershaw, R.; Uddin, S.; Bishop, S. M.; Welland, M. E. Understanding how charge and hydrophobicity influence globular protein adsorption to alkanethiol and material surfaces. *J. Mater. Chem. B* **2019**, *7*, 2349−2361.
(51) Beykal, B.; Herzberg, M.; Oren, Y.; Mauter, M. S. Influence of surface charge on the rate, extent, and structure of adsorbed Bovine Serum Albumin to gold electrodes. *J. Colloid Interf Sci.* **2015**, *460*, 321−328.
(52) Phan, H. T. M.; Bartelt-Hunt, S.; Rodenhausen, K. B.; Schubert, M.; Bartz, J. C. Investigation of Bovine Serum Albumin (BSA) Attachment onto Self-Assembled Monolayers (SAMs) Using Combinatorial Quartz Crystal Microbalance with Dissipation (QCM-D) and Spectroscopic Ellipsometry (SE). *PLoS One* **2015**, *10*, No. e0141282.
(53) Faucheux, N.; Schweiss, R.; Lutzow, K.; Werner, C.; Groth, T. Self-assembled monolayers with different terminating groups as model substrates for cell adhesion studies. *Biomaterials* **2004**, *25*, 2721−2730.
(54) McClary, K. B.; Ugarova, T.; Grainger, D. W. Modulating fibroblast adhesion, spreading, and proliferation using self-assembled monolayer films of alkylthiolates on gold. *J. Biomed. Mater. Res.* **2000**, *50*, 428−439.
(55) Okuyama, T.; Yamazoe, H.; Mochizuki, N.; Khademhosseini, A.; Suzuki, H.; Fukuda, J. Preparation of arrays of cell spheroids and spheroid-monolayer cocultures within a microfluidic device. *J. Biosci. Bioeng.* **2010**, *110*, 572−576.

https://dx.doi.org/10.1021/acs.biomac.0c01097
Biomacromolecules 2020, 21, 4857−4870